JOURNAL OF MATERIALS SCIENCE 12 (1977) 90–96

Adherence-fracture energy of a glass-bonded thick-film conductor: effect of firing conditions

P. F. BECHER, W. L. NEWELL*
Naval Research Laboratory, Washington, D.C., USA

The effect of firing conditions on the adherence of a glass-bonded Pt–Au printed thick film conductor to a 96 wt % Al_2O_3 substrate was determined by a fracture mechanics measurement of the critical fracture energy for catastrophic thick film–substrate separation. The technique also demonstrated that separation by slow crack growth (delayed failure) occurred in this system. Analysis of the thick film microstructure and fracture surfaces showed that optimum adherence was primarily a result of a mechanically interlocked interface formed between the conductor metal and the glass bonding layer which, in turn, was strongly bonded to the alumina substrate. The two step decrease observed in γ_{IC} (from 3.7 to 0.2 J m^{-2}) with firing temperatures over 860° C resulted from the removal of this interlocking metal–glass interface brought on by metal sintering and glass migration to the substrate. Thus, at 860° C firing temperatures, adherence is controlled by cohesive fracture in the glass bonding phase while above 1000° C it is controlled by adhesive failure of the weak chemical–physical bond at the metal–glass interface.

1. Introduction

Printed thick film microelectronic circuitry (e.g. conductors) often utilize a brittle glass or oxide phase to bond a metal conductor to a ceramic substrate. The adherence of such thick films (i.e. how strongly they are attached to substrates) is a function of the degree of interfacial bond formation and the thick film microstructure development during firing. Both can be quite dependent upon firing conditions and thus, as in other metallization systems [1–3], thick film adherence can be very process dependent [4].

Past studies of thick (or thin) film adherence to substrates have used peel-, tension- or bend-type loading conditions to obtain the load or stress to cause film separation (or fracture) from the substrate [4, 5]. Such data for fixed test conditions establish an adherence ranking. However, the tensile fracture stress, σ_f (or similarly the peel stress where thick film plastic deformation is limited), is dependent not only on materials properties but also on crack or flaw sizes, c, present, such that

$$\sigma_f = A(2E\gamma/c)^{1/2}$$

where E is Young's modulus of the material, γ is the material's fracture energy, and A is a geometric factor. This flaw size dependence of σ_f results in a rather tenuous correlation of adherence loads or stresses with materials or microstructural parameters.

On the other hand, such an analysis of adherence should be feasible with fracture mechanics techniques that quantitatively characterize crack propagation leading to thick film separation [6]. Such techniques have found extensive application in studies of the adherence of polymer adhesives [7–10] and most recently to ceramic–metal bonding [2, 3]. In the case of brittle or semibrittle bulk materials fracture the fracture energy, γ, is a measure of the energy for crack propagation in tension (catastrophic motion – γ_{IC}, or environ-

* Present address: Ceramic Engineering Department, Virginia Polytecnic Institute, Blacksburg, Va, USA.

© 1977 Chapman and Hall Ltd. Printed in Great Britain.

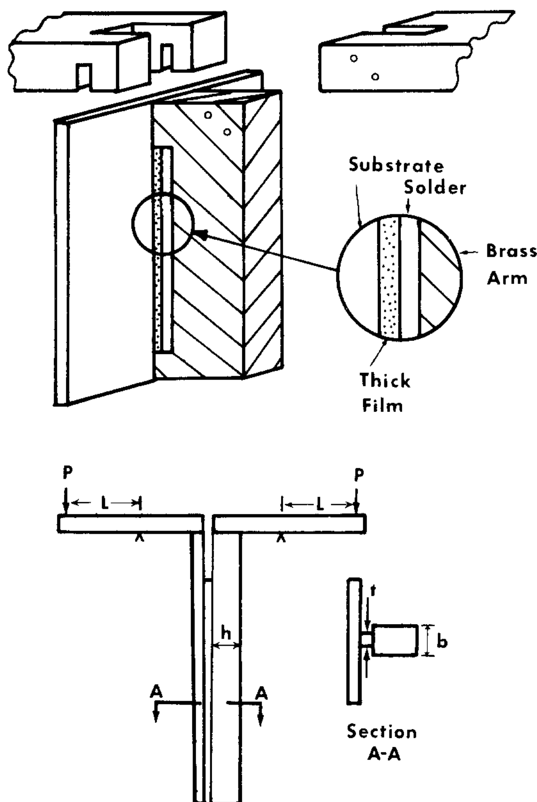

Figure 1 Applied moment double cantilever beam specimen for thick film adherence. Upper: actual specimen used for thick film showing load arm attachment and specimen cross-section. Lower: schematic drawing to indicate specimen dimensions and how bending moment (PL) is applied to specimen.

mentally sensitive slow crack growth – γ_I) and is a function of the material and its microstructure. The present study utilizing the fracture energy approach to adherence focuses on a glass-bonded Pt–Au conductor fired on 96 wt % alumina and the influence of the microstructure developed during firing.

2. Experimental

The fracture energy test used here to determine thick film adherence is a modification (Fig. 1) of the applied moment double cantilever beam technique [11]. This test has the advantage of not requiring crack length to determine γ. Because stiff loading arms are used, it also eliminates the plastic deformation of the pull arm found in peel tests.

The test specimens consisted of thick film strips (0.08 in. wide × 0.75 in. long) screen printed (200 mesh screen) on 96 wt % alumina substrates*, dried at 150° C for 15 min and fired in air to peak temperatures of 860 to 1100° C using the recommended firing profiles for the commercial Pt–Au conductor paste†. The test specimens were then dip soldered‡ in order to attach the brass cantilever arm. An alumina (0.05 in. thick × 1 in. × 1 in.) backing substrate was then added and the loading arms attached. Tests§ were run at 21° C, 40% r.h. in a universal machine¶ at a rate of $2 \times 10^{-2}\,\text{cm min}^{-1}$ for γ_{IC} values and at constant deflection conditions for γ_I values.

The fracture energy, γ, of the double cantilever beam specimen is obtained by equating γ to the change in stored strain energy in the cantilever arms of the specimen when fracture occurs. This change in stored strain energy, and thus γ, is based on the geometry of and the material in each cantilever arm. Thus for the thick film–substrate specimens, γ is obtained from the following equation:

$$\gamma = \tfrac{1}{2}\left[\frac{(PL)^2}{2t}\left(\frac{12}{E_1 b_1 h_1^3} + \frac{12}{E_2 b_2 h_2^3}\right)\right]$$

where PL is the applied moment (with P the load/arm, L the moment arm), b and h are the arm dimensions, and t is the thickness of the specimen at the crack plane (here the width of the thick film conductor line) with the subscripts 1 and 2 referring to the alumina and brass cantilever arms respectively (Fig. 1).

Post-fracture analysis of the two surfaces created by thick film separation included both optical microscopy and scanning electron microscopy/X-ray energy spectrometry techniques. This was coupled with observations of the microsturcture developed within thin layers of, and through the cross-section of, the thick film after

* AlSiMg 614 (1 in. × 1 in. × 0.025 in.) substrates, American Lava Corp., Chattanooga, Tenn, USA.

† Paste contains Pt and Au particles (average size ~ 0.5 μm and 2 μm), a high lead borosilicate glass with a Bi_2O_3 addition and an organic binder; E. I. Dupont, Wilmington, Del, USA.

‡ 63 Sn/37 Pb solder, 235° C for 30 sec using non-acid flux.

§ Sharp precracks required to determine γ_{IC} could be introduced by immersion of the specimen into liquid nitrogen; however, such precracking was not required as the data for precracked and unprecracked specimens fell within 10% of each other, evidence that sharp cracks already existed without the use of the liquid immersion.

¶ Instron Corp., Canton, Mass, USA.

10 min peak firings at temperatures of 860 to 1100° C. The latter were obtained by scribing the back surface of the substrate, then fracturing in liquid nitrogen so that the fracture surface contained both the substrate and the thick film.

3. Results and discussion

3.1. Thick film microstructures

As the thick film adherence was found to be dependent upon the microstructure developed within the film, this is discussed first. Such observations revealed that after the 860° C firing, the conductor consists of a very open Pt–Au network typified by neck formation between metal particles (initial stages of sintering). The glass in the thick film wets both this metal structure and the alumina substrate. As a result, progressing from the top of the conductor to the substrate, the thick film consists of three general layers: (1) a top layer in the form of an open metal network containing a glass coating, then (2) a glass matrix containing a metal network, and which changes to (3) a glass layer bonded to the substrate (e.g. Fig. 3).

After firing ⩾ 900° C, the conductor metal layer further densifies to form a more regular polycrystalline microstructure but still contains substantial continuous porosity (intermediate stage of sintering). The continuous porosity in the metal layer ranges from large ⩽ 1 mm diameter holes to ⩾ 10 μm diameter capillaries which are filled with glass. After firing ⩾ 1000° C, large regions of the conductor metal are fully densified with closure of the small diameter continuous porosity completed (final stage sintering). The overall metal layer is not continuous, as there are still large (~ 1 mm) holes through this layer. The glass layer still exists between the conductor and substrate (Fig. 4). There is now only limited glass coverage on the metal adjacent to the large holes in the conductor and no penetration of glass into the metal structure.

The formation of this glass layer between the conductor metal and substrate is a result of glass migration from the conductor onto the substrate. The ability of the glass to wet both the substrate and the Pt–Au acts as the driving force for glass migration. It is known that the contact angle for a similar lead borosilicate glass on the 96 wt % alumina substrate decreases from ~ 40° at 800° C to < 10° at 950° C after 10 min and contact angles for this glass on gold similarly decrease to ⩽ 10° at 950° C [12]. However, contact angles on platinum are still ⩾ 20° for PbO and B_2O_3 silicate glasses at temperatures up to 1180° C after 10 min [13]. Studies have shown that the contact angle for a borosilicate glass on platinum alloys increases with addition of a metal with high contact angle to one with a low contact angle [14]. Thus the glass would be most likely to have a contact angle on the Pt–Au metal between ~ 10° and ~ 20°. As a result, the glass would tend to migrate to the

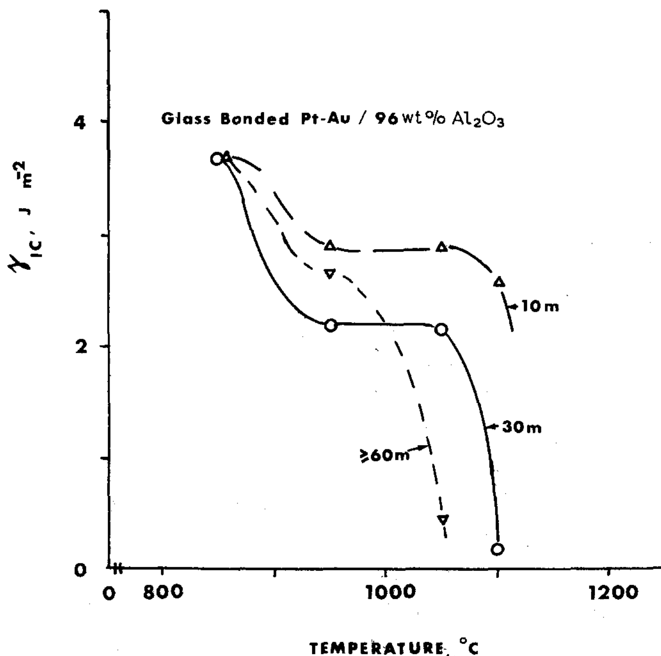

Figure 2 Critical fracture energy for thick film–substrate separation after various peak firing temperatures and times at peak temperature.

alumina substrate in order to lower its surface energy.

3.2. Catastrophic thick film separation

The γ_{IC} peak firing temperature data exhibited two features (Fig. 2): first, a small (~30%) decrease in γ_{IC} for firing temperatures of ~860° C, and second, a precipitous drop in γ_{IC} for firing temperatures $\geqslant$1000° C. By increasing the time at peak temperature the latter γ_{IC} drop is shifted towards lower peak firing temperatures.

Observations of both the substrate, A, surface and the conductor, B, surface created by the separation of the conductor from the substrate revealed the following. For the samples fired at 860° C, the A surface (substrate, Fig. 3a) consisted of a glass matrix with some metal particles while the B surface contained a metal network structure in a glass matrix (Fig. 3b). Thus, the macroscopic mechanically interlocked metal–glass interfaces as seen in the thick film microstructure (Section 3.1) leads to fracture in the glass layer (i.e. cohesive failure) between conductor and substrate (Fig. 3c). The observed γ_{IC} value (~3.7 J m^{-2}) is consistent with the 2 to 5 J m^{-2} values obtained with bulk glasses [15, 16] as compared to that of either aluminas (γ_{IC} = 15 to 25 J m^{-2}) or the much higher values for f c c metals and alloys. The included metal particles in the glass have little influence on γ_{IC} which is similar to the behaviour of bulk glass matrix–metal composites. On the other hand, some glass matrix–oxide particle composites exhibit increases in γ_{IC} over that of the parent glass [17].

For the samples fired at $\geqslant$1000° C ($\gamma_{IC} \geqslant 0.5$ J m^{-2}) the A surface (Fig. 4a) consisted of glass with a very smooth topography conspicuously devoid of fracture markings and often replicating the dense polycrystalline structure observed in the metal of the B surface (Fig. 4b). The fracture is now entirely along the metal–glass interface (Fig. 4c, adhesive failure) as there are no glass protrusions across the interface, which is consistent with the thick film microstructure (Section 3.1), to interact with the propagating crack. The low fracture energy values are consistent with either a weak physical interfacial bond due to intimate glass-to-metal contact or a weak chemical interfacial bond as suggested by a high glass-to-metal contact angle (Section 3.1). Both would be expected to lead to glass–metal interface (or adhesive) failure rather than cohesive glass fracture which requires more energy.

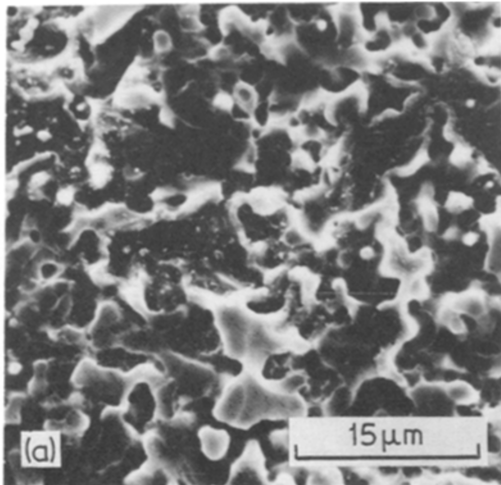

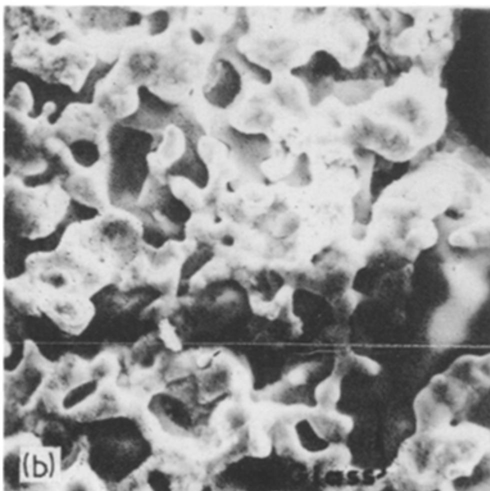

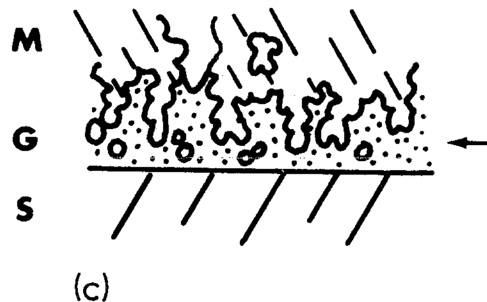

Figure 3 Fracture surfaces for thick film–substrate samples fired at 860° C. (a) Substrate side fracture surface exhibiting rough topography of glass layer including some individual metal particles. (b) Conductor side fracture surface showing lighter metal network in glass. (c) Arrow indicates locus of fracture plane in cross-section of samples (M, metal; G, glass; S, substrate).

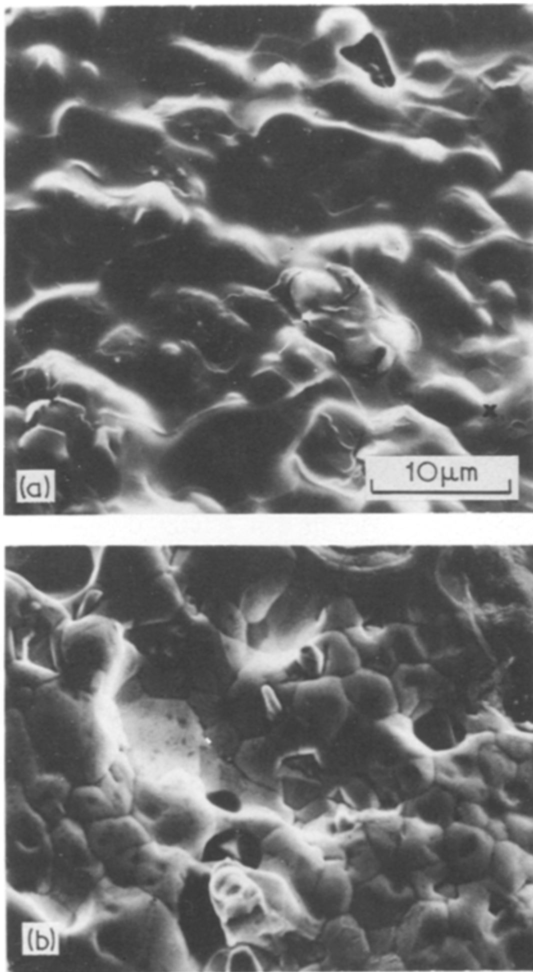

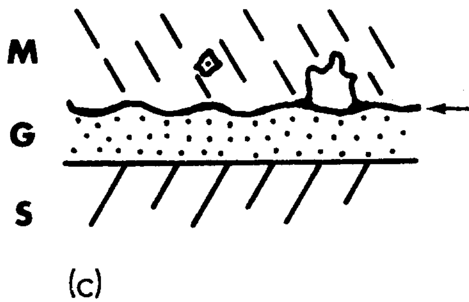

Figure 4 Fracture surfaces for samples exhibiting glass–metal interface (adhesive) separation. (a) Smooth glass layer on substrate with replications of metal grains (Note area at x). (b) Dense, polycrystalline metal at separated interface surface of conductor. (c) Locus of fracture plane in sample cross-section indicated by arrow.

For samples in the intermediate γ_{IC} and firing temperature range, the A surfaces were composed primarily of a glass matrix with an irregular topography which exhibited glass protrusions whose free surface ends had been broken off (Fig. 5a). The B surface (Fig. 5b) was composed of a polycrystalline metal matrix containing fractured glass fibrils. This interface, as seen here and through examination of the thick film structure (Section 3.1), has a microscopic interlocking structure. Fracture occurs at intermediate γ_{IC} values as the crack propagates along both the

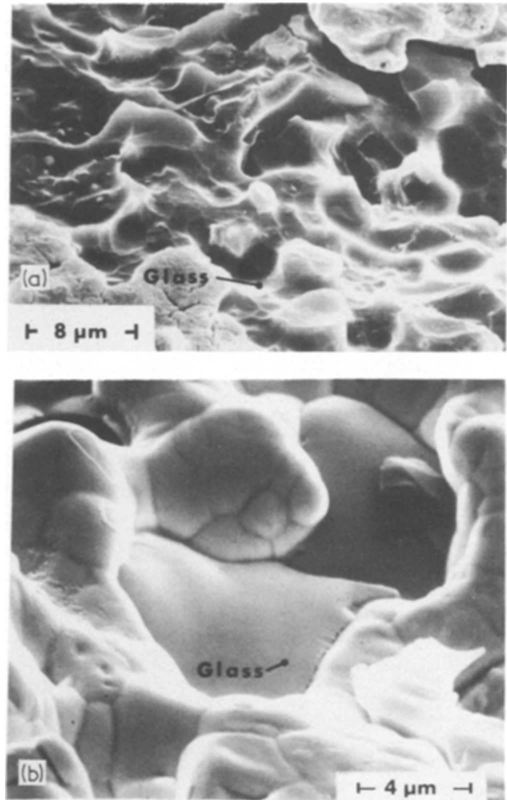

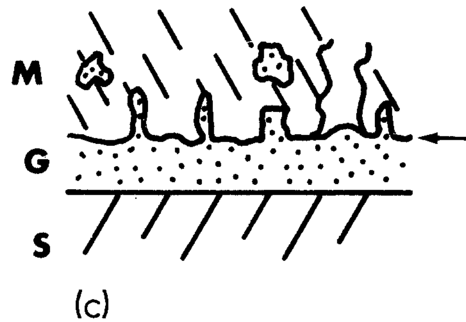

Figure 5 Fracture surfaces for mixed failure mode samples ($\gamma_{IC} \sim 2.5\ J\ m^{-2}$). (a) Fractured glass fibrals and regions of glass on substrate which exhibit replication of polycrystalline metal structure are seen. (b) Conductor surface composed of fractured glass fibrals in polycrystalline metal matrix. (c) Locus of fracture plane (arrow) in specimen cross-section.

TABLE I Critical fracture energy, γ_{IC}, for separating glass-bonded Pt/Au conductor from 96% Al_2O_3 substrate

Peak firing condition		γ_{IC}* ($J m^2$)	Number of specimens	Locus of separation
Temperature (°C)	Time (min)			
860	10	3.7 ± 1.6	21	Glass
	30	3.7 ± 1.5	7	
950	10	2.9 ± 0.5	4	Glass/glass–metal interface
	30	2.2 ± 1.0	4	
	60	2.7 ± 1.3	6	
	120	2.7 ± 1.6	14	
1050	10	2.9 ± 1.3	3	
	30	2.2 ± 0.6	4	
	120	< 0.5	3†	Glass–metal interface
1100	10	2.6 ± 0.6	6	Glass/glass–metal interface
	30	0.2 ± 0.1	6	Glass–metal interface

* Average ± S.D.

† Most specimens broke in handling; thus only an upper limit value shown.

interface and through glass fibrils which penetrate into the metal (Fig. 5c) giving rise to a mixture of adhesive and cohesive fracture.

The cause of the change in fracture mode from cohesive to adhesive failure and resultant lowering of γ_{IC} (Table I) is the removal of the interpenetrating (mechanical interlock) type of metal–glass interface as seen from the fracture surfaces and the thick film microstructure. The temperature–time dependence of this shift in fracture mode, as well as the observed thich film microstructural changes, indicate that continued metal sintering, which eliminates glass penetration into the metal and glass migration to the substrate, are the primary phenomena responsible for the altered interfacial microstructure.

3.3. Slow crack growth

A limited number of samples fired at 950° C for 60 min were subjected to fixed deflections such that the applied load was less than that required for catastrophic failure. With fixed deflection (loads equivalent to ~70% the critical load), the samples exhibited a slowly increasing rate of load loss after an initial incubation period (Fig. 6). This was terminated by a precipitous loss of load and separation of the conductor from the substrate. The observed behaviour is characteristic of slow crack growth phenomena, and the initial crack velocities were calculated to be $\sim 10^{-3}$ m sec^{-1} compared to $\sim 10^{-1}$ m sec^{-1} for the previous catastrophic fracture tests. The γ_I value for the initial slow crack growth was found to be ~ 1.7 J m^{-2} (i.e. less than γ_{IC} of 2.7, Table I) in keeping with the behaviour observed in glasses [18]. The observed slow growth is important as it shows that thick film separation from the substrate can occur at stresses less than that required for catastrophic separation by delayed failure. Times to failure under slow crack growth conditions are inversely proportional to the applied stress and are influenced by the environment (i.e. decreased by the presence of moisture).

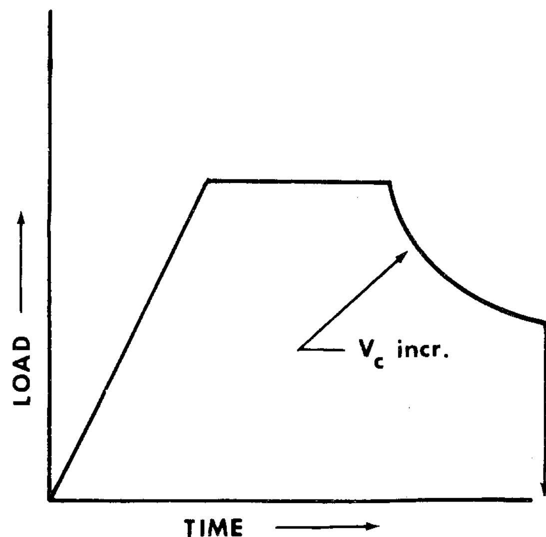

Figure 6 Schematic load–time curve for samples which exhibit slow crack growth. Samples were loaded to fixed deflection (constant load). After incubation period, load drop observed due to slow crack extension which was terminated by catastrophic crack extension.

5. Conclusions

(1) The peak firing time and temperature strongly influence the critical fracture energy, γ_{IC}, for thick film – substrate separation. A maximum in γ_{IC} is obtained when a macroscopic mechanical interlocked interface is formed between conductor metal and the glass layer formed on the substrate. Separation then occurs by fracture within this thick film glass phase (cohesive failure).

(2) The decrease in γ_{IC} for conductor separation with increased peak firing temperature and time is a result of conductor metal densification and glass migration which eliminate the mechanically interlocked nature of the glass–metal interface and leads to adhesive failure at the glass–metal interface.

(3) Slow crack growth is observed in samples in which glass phase fracture occurs and leads to time dependent failure at stresses below those required for catastrophic separation of the conductor from the substrate.

Acknowledgements

It is a pleasure to acknowledge helpful discussions of this work with R. W. Rice, S. W. Freiman, D. R. Mulville, W. D. Bascom and J. S. Murday of NRL, and T. T. Hitch and K. R. Bube of RCA Laboratories, as well as the work of L. A. Mann of NRL in the preparation of the thick film samples. The study was supported by the Naval Air Systems Command, J. W. Willis contract monitor.

References

1. M. E. TWENTYMAN, *J. Mater. Sci.* **10** (1975) 765.
2. G. ELSSNER, S. RIEDEL and R. PABST, *Pract. Metall.* **12** (1975) 235.
3. G. ELSSNER and R. PABST, *Proc. Brit. Ceram. Soc.* **25** (1975) 179.
4. T. T. HITCH, in Proceedings of the International Microelectronics Symposium, International Society for Hybrid Microelectronics, Montgomery, Alabama (1971) pp. 7–7.1–4.
5. B. N. CHAPMAN, *J. Vac. Sci. Tech.* **11** (1974) 106.
6. P. F. BECHER, W. D. BASCOM, J. L. BITNER, and J. S. MURDAY, in Proceedings of International Microelectronic Symposium, International Society for Hybrid Microelectronics, Montgomery, Alabama (1975) pp. 079–86.
7. S. J. BENNETT, K. L. DEVRIES, and M. L. WILLIAMS, *Int. J. Fracture* **10** (1974) 33.
8. E. J. RIPLING, S. MOSTOVOY, and H. T. CORTEN, *J. Adhesion* **3** (1971) 107.
9. E. J. RIPLING, S. MOSTOVOY, and C. BERSCH, *ibid* **3** (1971) 145.
10. W. D. BASCOM, C. O. TIMMONS, and R. L. JONES, *J. Mater. Sci.* **10** (1975) 1037.
11. S. W. FREIMAN, D. R. MULVILLE, and P. W. MAST, *ibid* **8** (1973) 1527.
12. K. R. BUBE and T. T. HITCH, Quarterly Technical Report No. 1, Contract Number N00019–75–C–0145 (NAVAIR), RCA Laboratories, Princeton, New Jersey, April 1975.
13. G. J. COPLEY and A. D. RIVERS, *J. Mater. Sci.* **10** (1975) 1291.
14. G. J. COPLEY, A. D. RIVERS and R. SMITH, *ibid* **10** (1975) 1285.
15. S. M. WIEDERHORN, *J. Amer. Ceram. Soc.* **52** (1969) 99.
16. J. J. MECHOLSKY, R. W. RICE and S. W. FREIMAN, *ibid* **57** (1974) 440.
17. D. R. BISWAS and R. M. FULRATH, *ibid* **58** (1975) 526.
18. S. M. WIEDERHORN, *ibid* **58** (1967) 407.

Received 13 April and accepted 26 May 1976.